Experimental and theoretical study of a differentially pumped absorption gas cell used as a low energy-pass filter in the vacuum ultraviolet photon energy range

B. Mercier, M. Compin, and C. Prevost
Laboratoire Pour l'Utilisation du Rayonnement Electromagnétique (LURE), bât 209D, Université Paris-Sud, BP38, 91898 Orsay Cedex, France

G. Bellec, R. Thissen,[a] and O. Dutuit[a]
Laboratoire de Chimie-Physique, bât 350, Université Paris-Sud, 91405 Orsay Cedex, France

L. Nahon[a),b]
CEA/DRECAM/SPAM, bât 522, CE de Saclay, 91191 Gif-sur-Yvette Cedex, France

(Received 28 February 2000; accepted 12 June 2000)

In order to separate the fundamental synchrotron radiation from the high harmonics emitted by an undulator, a low photon energy-pass filter has been designed and built, ensuring a high spectral purity on the vacuum ultraviolet (VUV) SU5 beamline at Super-ACO. It consists of an absorption cell filled with rare gases and separated from the ultrahigh vacuum of the storage ring and of the beamline by a double differential pumping obtained with thin capillaries. Its conception has been optimized by numerical computation of pumping speed. Admission pressures in the range of 100 Pa in the central part of the filter have been used without any degradation of the upstream or downstream ultrahigh vacuum. The measured attenuation factors above the energy cutoff are above 10^5 and 10^2 (and certainly above 10^3 with ultimate pressure of Ne) for argon and neon absorbing gases, respectively, with no measurable attenuation of fundamental radiation. A sophisticated numerical simulation of the pressure distribution, taking into account the geometry of the whole absorption cell including the first pair of capillaries, has been developed. The corresponding calculated attenuation factors are in very good agreement with the measurements, and thus allow reliable predictions of the expected attenuation factors for any given configuration of the filter. © *2000 American Vacuum Society*. [S0734-2101(00)07205-5]

I. INTRODUCTION

At the difference of laser lines which appear as discrete and uncorrelated lines in the spectrum, the synchrotron radiation (SR) has a specific spectral pattern: a broad white light continuum in the case of bending magnet sources, and in the case of insertion devices such as undulators, a spectrum consisting of a fundamental radiation with a series of harmonic peaks. In all cases SR-based sources are such that the radiation at frequency ω is associated to a series of harmonics: odd harmonics at 3ω, 5ω,..., as well as even harmonics depending on machine parameters and on the way that light is collected.[1] This is a problem when diffraction grating monochromators are used to monochromatize the SR coming from bending magnets or undulators, since the fundamental radiation and its harmonics are superimposed on the diffracted beam emerging from the exit slit, due to the nonzero higher order grating transmission. The presence of the transmitted harmonics can be a real problem since the signal they generate, as an ion or an electron yield for instance, can hide or overwhelm the signal produced by the fundamental radiation.

In order to overcome this high order/high harmonics contribution problem encountered with SR-based sources, several strategies can be followed: the main one, in the extreme ultraviolet range (above 40 eV), is the use of thin film filters. The material is chosen according to its absorption edge, so that the filter is transparent for the fundamental radiation and does not transmit the harmonics. For instance Al can be used with a typical thickness of a few 1000 Å with an absorption edge located at 72 eV, or Mg with an absorption edge at 49 eV,[2,3] and with a corresponding transmission factor in the range of several tens of percent. In the vacuum ultraviolet (VUV) range (5–40 eV) the situation is different and contrasted: while it is possible to use a silica solid window (up to 7.5 eV) or MgF_2 (up to 10.5 eV) or LiF (up to 11.8 eV) there is no transparent solid material above 11.8 eV.[4] Even below 11.8 eV, the use of solid material windows is not always fully satisfactory, especially in the LiF case, since there is still quite important absorption of the fundamental radiation itself, especially when the material has been exposed to the SR white light creating some strongly absorbing colored centers. The use of an optical bypass consisting of a set of plane mirrors placed at a variable grazing incidence could be considered[5] to cut the high energy photon contribution but with a rather low extinction ratio in the VUV range and, most of all, with an increasing complexity in terms of optics and mechanics. Finally, note that an alternative strategy for the future could consist, as it has been recently developed,[6,7] of using a specific state-of-the-art magnetic structure for undulators[8] to generate in some cases a spec-

[a)]Also with: LURE, bât 209D, Université Paris-Sud, BP38, 91898 Orsay Cedex, France.
[b)]Author to whom correspondence should be addressed; electronic mail: nahon@lure.u-psud.fr

trum with irrationally related frequencies of the harmonics. Such an approach is still under development and is not compatible with the fully electromagnetic versatile polarization capabilities that were required for the SU5 undulator of Super-ACO.[9]

For these reasons, in the VUV range, the use of a windowless gas cell, absorbing any photon whose energy is above the ionization potential of the filling gas, has been proposed and set up[10] on the Chemical Dynamics Beamline[11] at the Advanced Light Source (ALS). Based on a similar principle, we present here the harmonic filter which has been built on the SU5 VUV high resolution beamline[12] presently under final commissioning, and whose primary scientific goal deals with photon-induced dynamics involving the valence shells and chemical reactivity. These studies are very sensitive to the spectral purity of the photons deposited into the system. Starting with quite difficult conditions in terms of emittance, as encountered on second generation storage rings, we have built a very efficient gas filter with only two differentially pumped stages, instead of three for the ALS device, owing to the presence of long capillaries used as small conductance elements, whose geometry has been optimized by numerical simulations.

After the description of the constraints on the project and of the vacuum system necessary to fulfill them, the mechanical conception is briefly described. First experimental spectra, together with the related attenuation factors of the harmonics, obtained *in situ* with the SU5 undulator, are then presented and compared with simulations.

II. VACUUM AND MECHANICAL CONCEPTION

A. Constraints

In the conception of a gas filter for the undulator-based SU5 VUV beamline, there were several severe constraints necessary to achieve the task of suppressing high order/high harmonics components of the radiation.

(1) We wanted to cover a spectral range between 5 and 40 eV with at least three orders of magnitude of attenuation factor of the harmonics. Up to 8 eV, SiO_2 and MgF_2 windows will be used. Above, it is possible to fulfill this condition by using only two rare gases: argon and neon, which have an absorption edge around 15 and 20 eV, respectively. It is not necessary to use helium, as there is a negligible contribution of high order/high harmonics corresponding to a fundamental located between 20 and 24.6 eV (helium absorption edge), due to the suppression of energetic photons above 40 eV by absorption on the normal incidence optics of the beamline.

(2) We had to take into account the transverse characteristics of the emitted SR in the 5–40 eV photon energy range. The total diffraction-limited emission angle in the central cone around the undulator axis is typically 525 μrad at 5 eV and 215 μrad at 30 eV.[9] Let us note that the Super-ACO positron storage ring has a moderate emittance ($\varepsilon_x = 30$ nm rad, $\varepsilon_z = 15$ nm rad for the 24 bunch operation mode), so that the positron angular contribution can be neglected as compared to the undulator photon emission angle (it is exactly the opposite concerning the transverse size of the photon source, which is mostly limited by the positron beam emittance rather than by the photon diffraction limit). A general description of the undulator-based SU5 beamline can be found in Ref. 12. Briefly, at about 8 m from the center of the undulator, a toroidal mirror (M1) deflects and focuses the beam toward the center of the ring. The gas filter is designed to be installed at the focal point of this mirror, before the entrance slit of the monochromator. Optical ray-tracing simulations using the SHADOW code in the geometrical approximation with 2×2 mrad maximum total aperture show that the beam spot size is about 2 mm in diameter at the waist, increasing to about 3 mm at a distance of 675 mm (the distance at which the capillaries C3 and C4 are located). This rather big spot size corresponds to the total acceptance of the optics. However, as the actual opening angle of the SR emission lies in the submilliradian range, the use of conductance limiting capillaries having internal diameters slightly larger than 2 mm ensures a satisfactory optical transmission of the device.

(3) The budget allowed for the beamline construction was a severe constraint to optimizing the differential pumping of the gas filter, in particular the number of differential pumping stages and the choice of the type of pumps. In addition, the pumps had to be very reliable with an easy maintenance in order to minimize possible vacuum failures on the beamline.

(4) However, as higher harmonics intensity varies with K^2, the low K value ($K_{max}<3$) of the SU5 undulator gives much less intensity in the high order harmonics than the Chemical Dynamics Beamline undulator ($K=5.24$) at the ALS,[10] where a similar gas filter has been constructed.

(5) A very low partial pressure of the filling rare gases (typically about 10^{-10} Pa of argon) was allowed in the storage ring to avoid any decrease of the beam lifetime. The partial rare gas pressure had to be continuously monitored by quadrupole mass spectrometers both on the beamline and inside the storage ring.

B. Vacuum conception

In order to get an attenuation of the high harmonics by at least 3 orders of magnitude, a rough estimation using simply the Beer–Lambert law in the central region (see Fig. 1) shows that it is necessary to be able to have a rare gas pressure P_0 (argon or neon) of up to 100 Pa in the R1 absorption cell (see also Sec. III C). Differential pumping simulations show that it is possible to achieve such a pressure together with the fulfillment of the partial pressure constraints in the storage ring by using only two differentially pumped stages in the gas filter. between the R1 absorption cell and the R2 region, and between the R2 and R3 regions as seen in Fig. 1. The differential pumping between the R1 and R2 regions is obtained with two capillaries (C1 and C2) which have an internal diameter of 2.1 mm and a 10 cm length. Between the R2 and R3 regions, the capillaries (C3 and C4) have an inside diameter of 2.5 mm and the same 10 cm length. Their internal diameters are imposed by the beam spot size and the

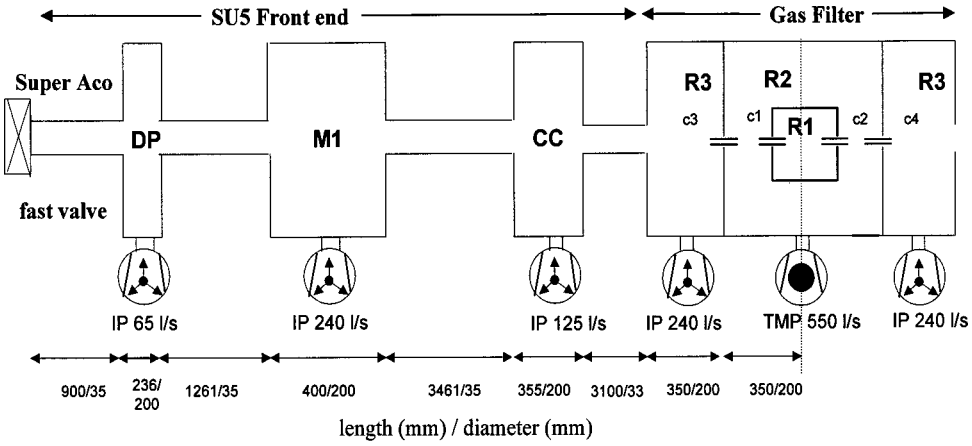

FIG. 1. Schematic of the SU5 beamline upstream part and of the gas filter. DP stands for the differential pumping stage protecting the ring vessel vacuum, M1 is the first SU5 mirror chamber, and CC is the calibration chamber in which the partial pressure of gas is measured owing to a quadrupole mass spectrometer. The bottom arrows indicate the different conductions length and diameter. IP stands for ion pump and TMP for turbomolecular pump.

length is chosen as the maximum value compatible with an easy alignment. With these capillaries, the total flux for argon as well as for neon is:

$$Q = 2C_t P_0 = 3.8 \times 10^{-3}\ \text{Pa m}^3/\text{s},$$

where C_t is the capillary conductance. In these two capillaries, the flow regime is intermediate and the downstream pressure is negligible as compared to the P_0 admission pressure (see the capillary pressure distribution in Sec. III). In the R2 region, it is possible to assume that the regime is molecular. In this case, the differential pressure distribution can be simulated by a computer code using the node model.[13] For each node, there is an equation such as

$$P_i \cdot \left[\left(\sum_k C_{k-i} \right) + S_i \right] - \sum_k P_k \cdot C_{k-i} = \sum_k \frac{Q_{k-i}}{2},$$

where k represents all the nodes around the i node, S_i the effective pumping speed at the i node, C_{k-i} the conductance between the i and k nodes, and Q_{k-i} the flux between the i and k nodes. A matrix resolution of these equations gives the pressure distribution of complex devices with distributed outgasing. Using an iterative calculation, the simulation takes into account the pumping speed dependence of the ion pumps as a function of the rare gas pressure. Figure 2 shows the pressure distribution calculated for a differential pumping from 100 Pa in the R1 cell to 10^{-10} Pa in the storage ring. it shows that the whole upstream part of the beamline is used to achieve the storage ring rare gas partial pressure requirement.

The R2 higher pressure region is evacuated by a hybrid turbomolecular pump which has a pumping speed of 550 l/s for nitrogen and argon. For the two R3 regions, «Starcell» type ion pumps 240 l/s (N_2) were chosen because of their higher pumping speed for rare gases (160 l/s for Ar) as compared to the classical ion pumps. Although turbomolecular pumps have higher pumping speed for rare gases, ion pumps were preferred over turbomolecular pumps because of their reliability and longer lifetime in the ultrahigh vacuum range. A pumping bypass was installed in the R3 region in order, in case of intensive use, to regenerate the two ion pumps once a week.

C. Mechanical design

Figure 3 shows a schematic of the gas filter mechanical design. It is composed of a L304 stainless steel chamber which has an internal diameter of 200 mm and a total length of 1264 mm, divided into three differentially pumped sections. Ultrahigh vacuum techniques are used, such as Conflat connection flanges (CFs). The gas cell section (R2) is closed at both ends by identical flanges equipped with *o*-ring

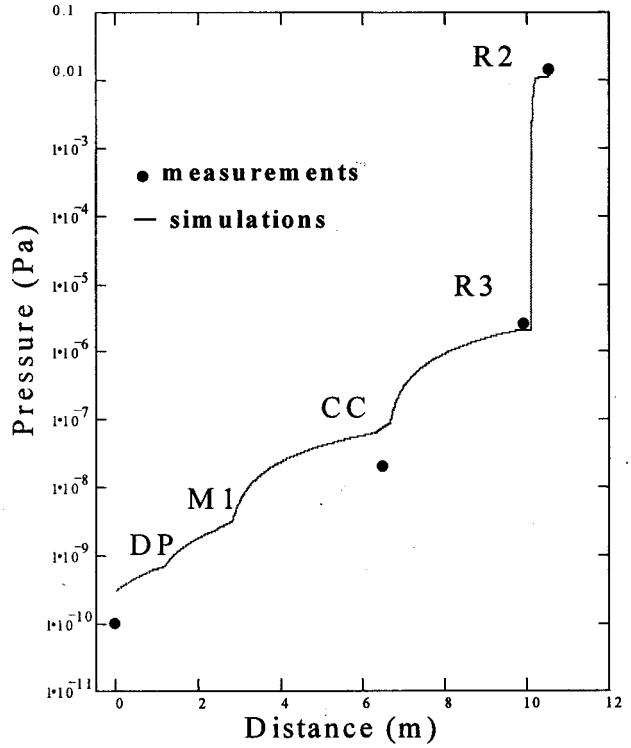

FIG. 2. Argon partial pressure distribution at different locations in the filter for an admission pressure of 100 Pa in region R1. The distances are referred to the fast valve between the storage ring and the beamline.

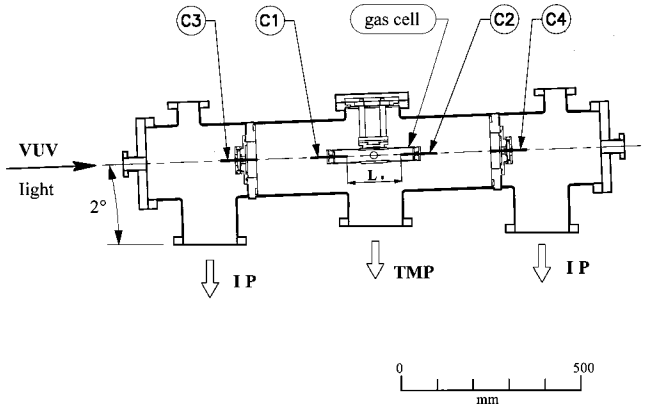

FIG. 3. Mechanical scheme (to scale) of the harmonic filter. C1–C4 represent the different capillaries.

mounted XY translation plate devices supporting the C3 and C4 capillaries. Three adjustment screws on each device allow the angular alignment of the capillaries. The gas cell is suspended in the center of the filter. Its internal diameter is 35 mm and its overall length is 220 mm. It is closed at both ends by two capillaries (C1 and C2), which are centered on a flange and mechanically coaxially aligned along the filter axis. Both capillary ends are cut at an angle of 45° to avoid reflections and any direct gas jet into the beamline. The distance between the C1 and C2 capillary ends in the gas cell (L_0) is 150 mm, corresponding to the effective absorption length in a first approximation. A DN16 stainless steel flexible tube connected to the gas cell ensures either its pumping when one changes absorbing gas or the gas load. A direct view of the light beam is made possible by a DN16 window located in the middle of the gas cell.

The filter chamber is connected to its stand by three screw jacks which are mounted on three translation plates designed for the X, Y, and Z alignment of the whole device on the beamline. The whole chamber is mounted on its stand with a 2° vertical angle as the light beam coming out of the M1 mirror.

The gas filter surfaces were first chemically cleaned, leak checked, and baked out previous to mounting on the beamline.

The different internal elements of the filter have been aligned before the implementation on the beamline site. The method consisted of aligning one-by-one each capillary by using both a cassitometer and a He–Ne laser, whose diffraction ring pattern was observed. Then the filter, considered as a whole entity, was aligned with the SR, in the air first, then under vacuum owing to a set of mirrors and windows reflecting the visible light produced by a ZnS fluorescent screen located at the upstream tip of the capillaries. The overall geometrical transmission of the filter with no gas is estimated to be above 50% as roughly measured from the spectrum of the undulator with a fundamental peak at 4.5 eV. Since the central cone of the undulator emission has an aperture scaling as the square root of the emitted wavelength, the transmission in the useful range of the filter (above 8 eV) should be higher. (It will be later on measured accurately with a calibrated photodiode).

III. EXPERIMENTAL RESULTS AND SIMULATIONS

A. Pressure distribution

Pressure measurements were performed in the different regions of the filter and the beamline using different gauge types, appropriate for the different pressure ranges; i.e. Pirani in R1, Pirani-Penning in R2, and Bayard Alpert (BA) in the chambers R3, calibration chambers (CC), M1, and differential pumping (DP). Two mass spectrometers gave access to the partial pressures at the level of the CC chamber, and the Super-ACO ring (see Fig. 1). Both the Pirani and the Pirani–Penning gauges were calibrated for argon, with a Baratron type gauge and a spinning rotor gauge. This calibration lowers the errors on absolute pressure measurements to within 5%. In the following, all pressures will be given as absolute.

As it can be inferred from Fig. 2, the targeted pressure distribution has been obtained in a satisfactory way. For the R2 and R3 chambers, when the ratio between rare gas partial pressure and outgasing pressure from the walls is larger than 10, measured values for argon and neon normalized for sensitivity factors are in very good agreement with simulations.

In the CC, M1, and DP chambers, the ''memory effect'' in the ionic pumps leads to an increase of total pressure measured with the BA gauge when the rare gas is introduced. In this case, the total pressure is not significant. Thus, the partial pressure in CC has been measured using a mass spectrometer. The ratio between simulation and measured values is around 3, probably due to nonabsolute calibration of the mass spectrometer. Inside the ring, up to the working pressure of 100 Pa of argon in R1, no significant signal was detected, which puts a maximum limit to the partial pressure of argon in these conditions of 10^{-10} Pa. When neon is loaded with the same pressure, the global efficiency of the differential pumping is lowered and a value of 4×10^{-10} Pa is estimated inside the ring. This different behavior is due to the higher conductance of neon in the molecular regime.

The CC mass spectrometer, providing it has significant partial pressures, is interfaced as an active part of the security system of the beamline, as well as the Pirani gauge of the R1 chamber. Both have the effect of closing fast valves preventing the gas from escaping beyond the R3 chambers, when the rare gas pressure exceeds a preset value.

B. Experimental spectra

In order to establish the filtering efficiency of the whole device, before mounting the actual SU5 monochromator, we installed a testing setup at the exit of the filter. This setup was centered around a toroidal grating monochromator with a 0.30 m focal length (Jobin–Yvon HT30) equipped with a Pt-coated 550 grooves/mm grating blazed around 40 eV. The monochromatized beam emerging from the exit slit was collected on a fluorescent screen (a methylsalicylate surface), converting the VUV photons into visible photons, which were detected by a photomultiplier. With the setting of both

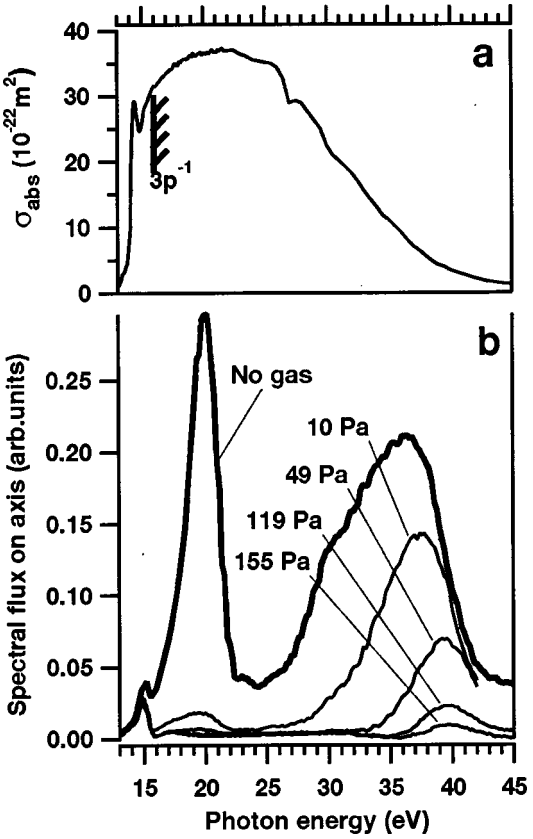

FIG. 4. (a) Absorption spectrum of Ar with absolute cross sections from Ref. 14 convolved with our spectral bandwidth. (b) First and second harmonic spectrum of the undulator for different admission pressures of Ar in the filter.

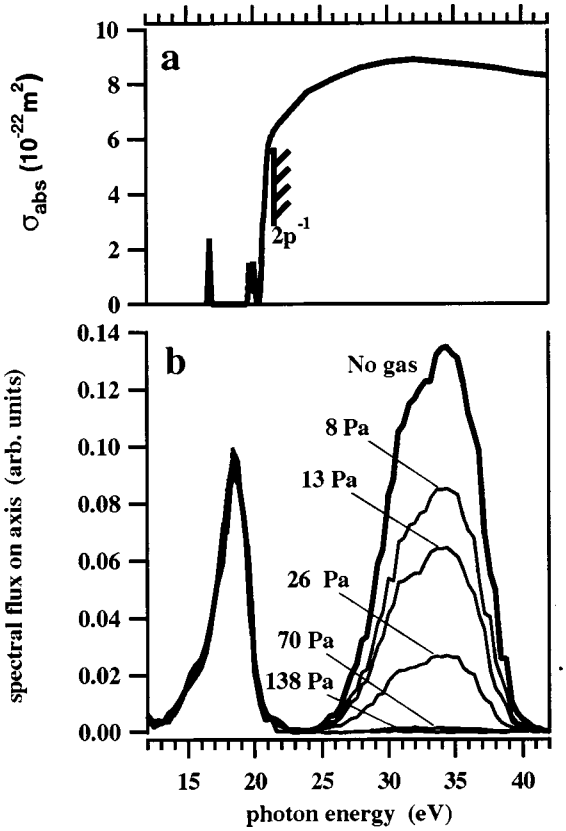

FIG. 5. (a) Absorption spectrum of Ne with absolute cross sections from Ref. 15 convolved with our spectral bandwidth. (b) First and second harmonic spectrum of the undulator for different admission pressures of Ne in the filter.

slits to 1000 μm, the typical resolution of this monochromator is about 600 meV full width half maximum at 15 eV photon energy. This relatively poor resolving power was inherent to the testing setup as the entrance slit of the monochromator was not set at a focal point and therefore had to be opened widely to collect a sufficient amount of photons without introducing any radiation collecting angular effects. However, concerning filtering efficiency and absorption edge determination, this resolution was sufficient enough to collect meaningful data.

Because of the nonperfect alignment of the light baffles inside the monochromator, some light due to total reflection on the grating (zero order) was still visible in the recorded spectra. This signal appears as a background, smoothly increasing with photon energy (the geometrical position of zero order corresponding to an infinite energy for a given value of the grating rotation angle). We removed this contribution from the spectra, assuming an exponential increase of this zero order signal in the considered energy region. As seen in the spectra presented in Figs. 4(b) and 5(b), the result of this correction leads to almost flat background for highly filtered signals, which leads us to believe that the procedure is valid, and that the only signal visible in Figs. 4(b) and 5(b) is due to VUV light, without pollution from extended zero order.

Figure 4 corresponds to the filtering efficiency measurements performed for argon as an absorbing gas. The uppermost part of the figure shows the evolution of the absorption cross sections of argon as a function of photon energy as given from Ref. 14, convolved with the spectral bandwidth of our monochromator. This absorption spectrum presents a sharp increase at 15 eV, corresponding to the absorption of photons by neutral atomic states converging toward the ionization edges (at about 15.8 eV). It is then slightly constant around a value of $30\times10^{-22}\,\mathrm{m}^2$ up to 28 eV, and then decreases to reach almost zero for 45 eV photon energy. From this curve, one can assume that the filtering efficiency of argon should be very high for photon energies located between 15 and 28 eV (which is the harmonics energy range in which we plan to use this gas). However, for the purpose of calibration, the almost linear decrease in absorption efficiency for higher photon energies is a very good test of the sensitivity of our measurements, since for those energies, nontotal extinction of the signal can be expected.

For the measurements presented in Fig. 4, and according to the previous statement, the first harmonic of the undulator was set at a value of 20 eV in order to have a maximum photon intensity available in the energy region close to the absorption edge of argon. As the second harmonic of the undulator, located at 40 eV, is still intense this gave us the opportunity to check the efficiency of the filter for lower absorbing efficiency of argon. Results are presented for five

different pressure conditions, ranging from ''no-argon'' in the filter up to 155 Pa, the highest authorized admission pressure in terms of the corresponding partial pressure in the storage ring vacuum vessel. One can clearly see that already for the lowest introduced argon pressure of 10 Pa, the first harmonic signal is drastically reduced for photon energies between 15 and 22 eV, while the second harmonic signal, corresponding to lower absorption cross sections, presents a much less drastic reduction. Moreover, the higher the photon energy, the lower the intensity reduction. This leads, when increasing the argon pressure, to the clear displacement of the maximum of the second harmonic. These measurements on the second harmonic were very useful in order to extract attenuation factors in the range of 10^{-5} as they gave us the opportunity to measure the absorption efficiency of the filter for high argon pressures leading to almost total extinction of the first harmonic, for which no valid measurement could be performed.

Figure 5 corresponds to the filtering efficiency measurements performed for Ne as an absorbing gas. The uppermost part of the figure shows the evolution of the absorption cross sections of Ne as a function of photon energy as given from Ref. 15, convolved with the spectral bandwidth of our monochromator. This absorption presents some discrete structures at 17 and 19.5 eV and a sharp increase at 20 eV, corresponding to the absorption of photons by neutral atomic states converging to the ionization edges (at about 21.5 eV). The absorption then varies slightly around a value of $7 \times 10^{-22}\,\mathrm{m}^2$ in the whole energy range. Let us note that the maximum absorption efficiency of argon is more than four times larger than that of Ne, which lets us predict a slightly lower efficiency of the filter when loaded with Ne. However, as seen above, the behavior of Ar is excellent in the energy range of 15–28 eV, and still satisfactory up to 32 eV, which restricts the necessity of using neon as the filtering gas to the only experiments requiring photon purity of the fundamental radiation between 15 and 20 eV.

For the measurements presented in Fig. 5(b), the first harmonic of the undulator was set to a value of 17.5 eV and this fixed the second harmonic of the undulator to 35 eV right in the useful absorption range of neon. This first harmonic energy was chosen in order to determine the eventual decrease of transmission in the filter, which could be due to some diffusion processes, appearing at high loading pressures. Results are presented for six different pressure conditions, ranging from ''no neon'' in the filter, to the highest admission pressure of 138 Pa. One can clearly see that the intensity of the second harmonic decreases regularly when pressure increases. When increasing the pressure from 70 to 138 Pa, one can still observe a slight decrease in the transmitted light, then falling within the noise level, preventing us from performing reliable measurements for higher pressures.

One can also see in Fig. 5(b) that for the photon energies located below the absorption edges (21.5 eV), there is no variation of the transmitted light intensity, i.e., negligible scattering, which shows another advantage of this type of filter: providing high purity of photons without loss in intensity.

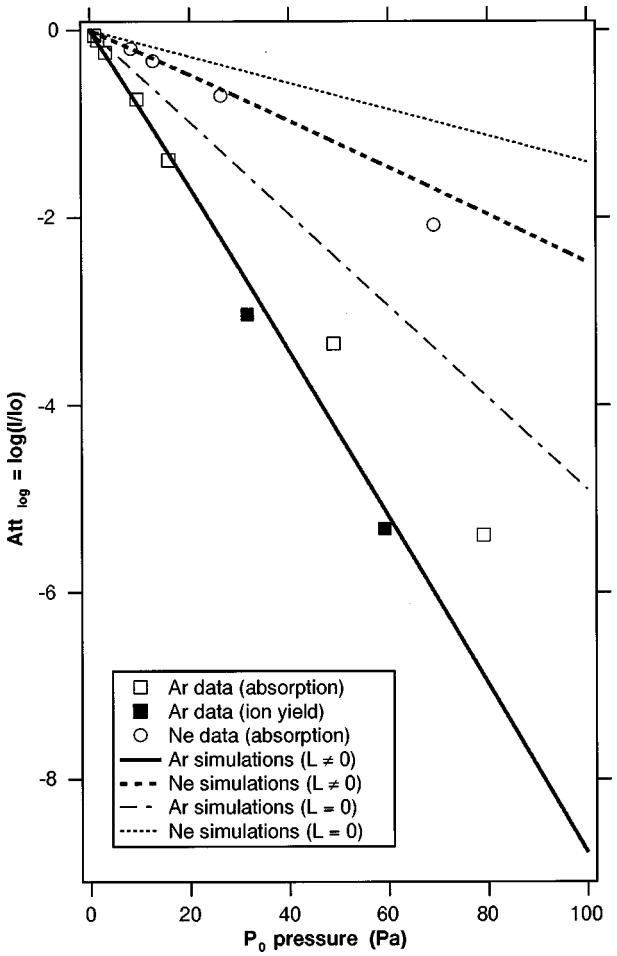

FIG. 6. Measured and calculated total logarithmic attenuation factor of the high pressure cell as a function of the admission pressure P_0 in region R1 for argon and neon used as filling gases and measured at 16 and 35 eV, respectively. The simulation referred to as ''$L \neq 0$'' takes into account the whole geometry of the absorption cell including the first pair of capillaries.

C. Attenuation factors

In this section we will derive the attenuation experimental factors of the harmonics, above the absorption edge of the filling gas, and compare them with numerical simulations in order to get a quantitative understanding of the general filter concept and its capabilities.

1. Measurements

Experimental attenuation factors were extracted from a series of spectra corresponding to Figs. 4 and 5 (which present only a few relevant spectra, from a larger series). They are based on a direct measurement of the decreasing transmitted photons with increasing admission pressures and correspond to the so-called ''absorption data'' in Fig. 6. In order to extract numerical values, we took the ''no gas'' spectrum as a reference, or I_0 signal, and then measured, for

a given photon energy, the intensity transmitted for each filling pressure I. Attenuation is then simply the logarithmic value of the ratio I/I_0.

In the case of argon, this procedure was applied at two photon energies, 16 and 37 eV, which provided us with an extended sensitivity as the absorption of argon at 37 eV is strongly reduced. Values extracted for 37 eV were normalized to an equivalent absorption at 16 eV by applying a correction factor corresponding to the ratio between absorption cross sections of argon at 16 and 37 eV to the derived logarithmic value [see Eq. (6) for formalism]. In the case of neon, the procedure was applied at 35 eV, corresponding to the maximum of the second harmonic.

In all cases, it is clear that the difficulty in the extraction of numerical values is limited by the ability to accurately determine the ''total extinction level,'' and this is especially the case for high pressure measurements. We estimate that the error bars associated to these measurements increases as a function of pressure, to reach a value larger than 1 order of magnitude for the maximal pressure used for both gases.

In order to increase the precision in the attenuation factor measurements at high admission pressures we performed, in the case of argon, some ion yield spectroscopy with the actual 6.65 m SU5 monochromator. It consists of measuring the number of mass-selected Ar^+ ions ($m=40$) produced by 16 eV photons on an effusive jet of argon located in a gas-phase experimental chamber positioned after the monochromator, for different admission pressure of Ar in region I of the filter (no gas, 32, and 59 Pa). The corresponding values of the attenuation factors are reported in Fig. 6. As the 6.65 m monochromator has much less stray light than that of the 0.3 m, we could directly measure at 16 eV an attenuation of more than 195 000 (log value of -5.32) for 59 Pa of Ar in the filter, in a reliable manner.

2. Simulation of the pressure distribution in a capillary

Before computing the simulated attenuation factors we present here the modelization of the pressure distribution in a capillary, $P(x)$. The flow regime in a capillary is determined by comparing the mean free path of the gas with the capillary internal diameter. In our case, with admission pressures ranging from 0.1 to 100 Pa and a diameter of 2.1 mm, the three regimes, i.e., molecular, intermediate, and laminar, can be encountered and should be considered.

The general expression of the total conductance C_T of a circular section long capillary (length $\gg$ diameter) is given by

$$C_T = C_L + Z \cdot C_M, \tag{1}$$

where C_L and C_M are the conductances in the laminar and molecular regimes, respectively, and Z is the empirical factor determined by Knudsen.[16] This can be rewritten as follow:

$$\mathbf{C_T} = \frac{\mathbf{A}\cdot\overline{\mathbf{P}} + \mathbf{B}\cdot\left(\frac{1+\mathbf{C}\cdot\overline{\mathbf{P}}}{1+\mathbf{D}\cdot\overline{\mathbf{P}}}\right)}{\mathbf{L}}, \tag{2}$$

with $A=2.86\times10^{22}\cdot\rho^2\cdot(M\cdot T)^{-1/2}\cdot\phi^4$, $B=1.2\cdot(T/M)^{1/2}\cdot\phi^3$, $C=4\times10^{23}\cdot\rho^2/T\cdot\phi$, and $D=5\times10^{23}\cdot\rho^2/T\cdot\phi$, where ρ is the atomic diameter, M the molar mass, T the temperature, R the ideal gas constant, ϕ the capillary diameter, L its length, and P the average pressure (all these quantities being expressed in the International System Units).

The flux Q is conserved over the whole capillary length so that, if one considers a small element of this capillary dx, one gets

$$Q = \delta C_T \cdot dP = \frac{A\cdot P(x) + B\cdot\left(\frac{1+C\cdot P(x)}{1+D\cdot P(x)}\right)}{dx}\cdot dP. \tag{3}$$

The integration of Eq. (3) yields

$$\frac{\mathbf{A}}{2}\cdot\mathbf{P}(\mathbf{x})^2 + \frac{\mathbf{B}\cdot\mathbf{C}}{\mathbf{D}}\cdot\mathbf{P}(\mathbf{x}) + \frac{\mathbf{B}\cdot(\mathbf{D}-\mathbf{C})}{\mathbf{D}^2}\cdot\ln(1+\mathbf{D}\cdot\mathbf{P}(\mathbf{x})) = -\mathbf{Q}\cdot\mathbf{x}+\mathbf{K}, \tag{4}$$

where K is an integration constant. A numerical solving of this equation shows that the third term on the left-hand side of Eq. (4) can be neglected with less than 3% error on the SR attenuation factors. The boundary conditions $P(0)=P_0$ (admission pressure) and $P(L)=P_L$ (pressure at the exit of the capillary) allow us to express the K and Q constants as a function of P_0 and P_L.

The P_L pressure can be determined for two extreme cases.

Case 1. One supposes that the gas cannot move faster than the speed of sound and that the expansion is isotherm, so that

$$P_L = (4K/L)/(\pi\phi^2 U),$$

where U is the speed of sound.

Case 2. One supposes that the flow regime is molecular and that the pressure is given by the pressure at the turbopump level (region 2) with an effective pumping speed S (177 l/s), so that

$$P_L = P_0/(1+S/C_T).$$

In both cases, solving Eq. (4) without the logarithmic term yields a pressure distribution that can be expressed as

$$\mathbf{P}(\mathbf{x}) = \mathbf{K}_0 + (\mathbf{K}_1 - \mathbf{K}_2\mathbf{x})^{1/2}, \tag{5}$$

where $K_0=-(B^*C)/(A^*D)$, $K_1=(K_0-P_0)^2$, and $K_2=2Q/A$.

Figure 7 shows the pressure distribution along the C1 and C2 capillaries in the case of argon, at 293 K, and for an admission pressure P_0 of 100 Pa. In such a case the flow regime is intermediate with a conductance $C_T=1.86\times10^{-2}$ l/s. Whatever the admission pressure (ranging from

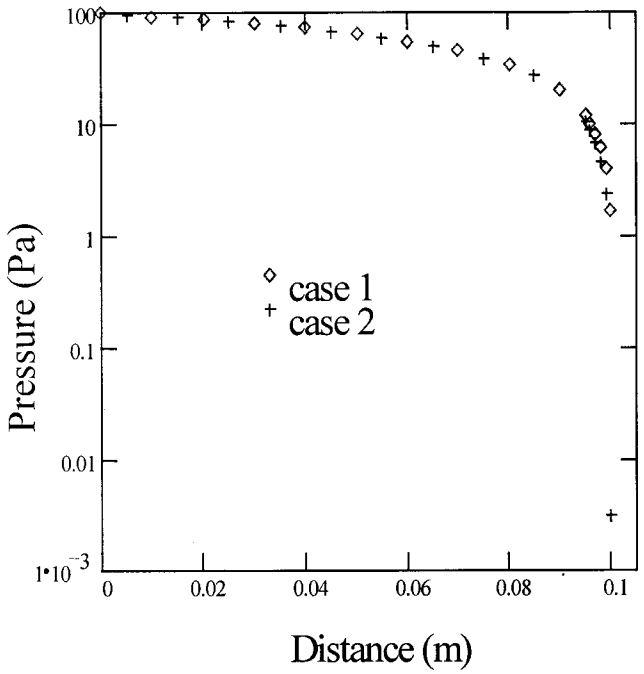

FIG. 7. Pressure distribution in the capillary as calculated from Eq. (5), in case 1 and case 2 approximations for the determination of the end capillary pressure P_L.

1 Pa to a few 100 Pa), one can consider with a negligible effect that the two cases are equivalent for the calculation of the attenuation factors. In the following, we will take the case 2 approximation.

3. Simulated attenuation factors and comparison with the experiment

We are now able to derive the simulated attenuation factors in one of the capillaries starting from the well-known Beer–Lambert law for absorption. The application of this law is relevant since, as it has been emphasized in Sec. III B, the scattering processes can be neglected in our experimental conditions, so that

$$dI = -I(x)\cdot\sigma_{\mathrm{abs}}\cdot n(x)\cdot dx, \tag{6}$$

where $I(x)$ is the photon flux, $n(x)$ the particle density at the position x in the capillary, and σ_{abs} the absorption cross section at the considered photon energy. In the case of an ideal gas, the density $n(x)$ can be expressed as $n(x)=P(x)/kT$, where k is the Boltzmann constant.

By taking the expression of $P(x)$ as given by Eq. (5), one can easily solve Eq. (6), with an integration constant set by considering the attenuation due to the central part of the absorption cell of length L_0 with a uniform pressure P_0. Considering in addition the geometry of the complete absorption cell, with a central part (length L_0) located in between the two C1 and C2 capillaries (length L), one gets a logarithmic attenuation $\mathrm{Att}_{\log}$ given by

$$\mathrm{Att}_{\log} = \log\left(\frac{I}{I_0}\right) = -\frac{2\sigma_{\mathrm{abs}}}{kT\ln(10)} \times\left(K_0 L - \frac{2}{3}\frac{(K_1-K_2L)^{3/2}}{K_2} + \frac{1}{2}P_0L_0 + \frac{2}{3}\frac{(K_1)^{3/2}}{K_2}\right). \tag{7}$$

Note that here we have neglected the absorption due to the medium and low density stage of the filter (R2 and R3, respectively). In practice, the total logarithmic attenuation of the filter, at 20 °C, as a function of the absorption cross section $\sigma_{\mathrm{abs}}\,(\mathrm{m}^2)$ of the filling gas with an effective atomic diameter $\rho(\mathrm{m})$, and as a function of the admission pressure $P_0\,[\mathrm{Pa}]$ can be expressed as

$$\mathbf{Att}_{\log} = \log\left(\frac{\mathbf{I}}{\mathbf{I_0}}\right) = -2.15\times10^{20}\sigma_{\mathrm{abs}}\mathbf{P}_0 \times\left(\frac{0.141\mathbf{P}_0 + 1.17\times10^{-18}\rho^{-2}}{\mathbf{P}_0 + 9.37\times10^{-18}\rho^{-2}}\right). \tag{8}$$

The corresponding light attenuation, labeled ''$(L\neq0)$'', is plotted in Fig. 6 as a function of P_0 in the case of argon and neon with an effective diameter of 3.67 Å for argon and 2.60 Å for neon[17] and an absorption cross section for argon at 16 eV of 30.4 Mbarn ($30.4\times10^{-22}\,\mathrm{m}^2$)[14] and for neon at 35 eV of 8.75 Mbarn ($8.75\times10^{-22}\,\mathrm{m}^2$).[15] The agreement between the experimental results by direct absorption and the simulation is very satisfactory, especially in the low pressure range. In the higher pressure range, there are some discrepancies whose origin may lie in the gauge calibration, turbulent behavior, or nonperfect behavior of gases, but is most probably due to the difficulty of estimating the residual part of transmitted light after passing through the filter, as for those high pressures, the signal becomes comparable to the noise level. This is why for the high pressure range in the case of Ar, the ion yield measurements at 32 and 59 Pa, less affected by this signal-to-noise limitation, should be considered as the most reliable data whose agreement with the numerical simulation is excellent.

This clearly demonstrates not only the validity of the pressure distribution calculations but also the necessity of such a sophisticated approach. Indeed, as it can be seen in Fig. 6, the rough approximation consisting of considering only the attenuation due to the central part of the absorption cell (length L_0) and neglecting the capillaries, i.e., setting $L=0$ in Eq. (7), leads to predictions in very poor agreement with the measured values.

Finally, note that in the case of neon, we could not extract a reliable experimental value for an admission pressure of 138 Pa, but that the corresponding theoretically predicted value is above 1000, fulfilling the requirement of Eq. (1) exposed in Sec. II A.

IV. CONCLUSIONS

We have conceived and built a very efficient low-energy pass filter ensuring a high spectral purity of the photons delivered by the VUV SU5 beamline. Owing to numerical simulations of differential pumping speed, the design has been optimized in terms of targeted performances and cost, leading to acceptable partial pressures in the storage ring vacuum vessel with up to 155 Pa of Ar and 138 Pa of Ne. The measured attenuation factors above the energy cutoff are above 10^5 and 10^2 (and certainly above 10^3 with ultimate pressure) for argon and neon absorbing gases, respectively, with no measurable attenuation of the number of photons whose energy is located below the cutoff. In very good agreement with the measured values a sophisticated numerical approach, taking into account the geometry of the whole absorption cell including the first pair ofcapillaries and not only its central part, has been developed. It allows reliable predictions of the expected attenuation coefficients for any given configuration of the filter in terms of the nature of the filling gas, the admission pressure, and the photon energy to be filtered. Finally, note that on a low emittance third generation synchrotron source, this filtering device could be much more efficient since it would be possible to use much thinner capillaries allowing a much higher admission pressure in the central part.

ACKNOWLEDGMENTS

The authors would like to thank the technical staff of the Laboratoire pour l'Utilisation du Rayonnement Electromagnétique (LURE), and especially the storage ring vacuum group. C. Depautex is warmly acknowledged for his involvement in the design of the filter as well as A. G. Suits and P. Heimann for helpful discussions.

[1]See for instance K. J. Kim, AIP Conf. Proc. **184**, 565 (1988).
[2]J. A. R. Samson, *Techniques of Vacuum Ultraviolet Spectroscopy* (Wiley, New York, 1967).
[3]F. R. Powel and J. R. Fox, Proc. SPIE **2011**, 428 (1993).
[4]C. Kunz, *Synchrotron Radiation Techniques and Applications* (Springer, Berlin, Germany, 1979), pp. 100 and 102.
[5]J. Underwood, E. Gullikson, M. Koike, and P. J. Batson, Proc. SPIE **3113**, 214 (1997).
[6]J. Chavanne, P. Elleaume, and P. van Vaerenbergh, *Proceedings of the European Particle Accelerator Conference 1998, 22–26 June, Stockholm, Sweden* (Institute of Physics, Bristol, 1998), pp. 2213 and 2215.
[7]B. Diviacco, R. Bracco, D. Millo, D. Zangrando, and R. Walker, *Proceedings of the European Particle Accelerator Conference 1998, 22–26 June, Stockholm, Sweden* (Institute of Physics, Bristol, 1998), pp. 2216 and 2218.
[8]S. Hashimoto and S. Sasaki, Nucl. Instrum. Methods Phys. Res. A **361**, 611 (1995).
[9]L. Nahon, M. Corlier, P. Peaupardin, F. Marteau, O. Marcouillé, P. Brunelle, C. Alcaraz, and P. Thiry, Nucl. Instrum. Methods Phys. Res. A **396**, 237 (1997).
[10]A. G. Suits, P. Heimann, X. Yang, M. Evans, C. W. Hsu, K. T. Lu, Y. T. Lee, and A. H. Kung, Rev. Sci. Instrum. **66**, 4841 (1995).
[11]P. A. Heimann *et al.*, Proc. SPIE **2856**, 90 (1996).
[12]L. Nahon, B. Lagarde, F. Polack, C. Alcaraz, O. Dutuit, M. Vervloet, and K. Ito, Nucl. Instrum. Methods Phys. Res. A **404**, 418 (1998).
[13]Y. Saito, M. Kakihara, and G. Horikoshi, J. Vac. Sci. Technol. A **12**, 1648 (1994).
[14]W. F. Chan, G. Cooper, G. R. Burton, and C. E. Brion, Phys. Rev. A **46**, 149 (1992).
[15]J. M. Bizau and F. Wuilleumier, J. Electron Spectrosc. Relat. Phenom. **71**, 205 (1995).
[16]R. Gordon Livesey, in *Foundation of Vacuum Science and Technology*, edited by J. M. Lafferty (Wiley, New York, 1998), p. 129.
[17]B. B. Dayton, in *Foundation of Vacuum Science and Technology*, edited by J. M. Lafferty (Wiley, New York, 1998), p. 39.